CFD analysis of 10-MW wind turbines

Vladimir Leble, Yaxing Wang, George Barakos
University of Liverpool, L69 3GH, Liverpool, United Kingdom (G.Barakos@liverpool.ac.uk)

Summary

This paper presents results of numerical computations for two 10-MW wind turbines. The aerodynamic loads and blade deformations are computed using the Helicopter Multi-Block (HMB2) flow solver developed at University of Liverpool. HMB2 solves the Navier-Stokes equations in integral form using the arbitrary Lagrangian-Eulerian formulation for time-dependent domains with moving boundaries. In this work, the blades are treated as rigid or elastic. Further, both 10MW designs were equipped with actuated leading and trailing edge flaps located at 60%R and 75%R. The obtained results show the potential of the actuated flaps to change the span-wise distribution of blade loads.

1. Introduction

To maximise the amount of produced energy, wind turbine rotor diameters have recently increased reaching values of 160m. Therefore, large scale wind turbines are operating at high Reynolds numbers and at high tip speeds, where compressibility effects begin to be important. In this paper, results from CFD analyses of 10-MW wind turbines are shown. The Helicopter Multi-Block (HMB2) solver developed at Liverpool University [1] is used to estimate the aerodynamic forces and blade deformation. The HMB2 solver has so far been validated for several wind turbine cases, including the NREL Annex XX [2] and Mexico project [3] experiments. Two 10-MW wind turbines are used in this work, named InnWind [4] and AVATAR [5]. Their rotors have diameters of 178.3m and 205.8m, respectively.

2. Numerical methods

The HMB2 code is a 3D multi-block structured solver and solves the Navier-Stokes equations in the 3D Cartesian frame of reference. HMB2 solves the Navier-Stokes equations in integral form using the arbitrary Lagrangian-Eulerian formulation for time-dependent domains with moving boundaries. The solver uses a cell-centred finite volume approach combined with an implicit dual-time method. Osher's upwind scheme is used to resolve the convective fluxes. Central differencing (CD) spatial discretisation method is used to solve the viscous terms. The non-linear system of equations that is generated as a result of the linearisation is then solved by integration in pseudo-time using a first-order backward difference method. A Generalised Conjugate Gradient (GCG) method is then used in conjunction with a Block Incomplete Lower-Upper (BILU) factorisation as a pre-conditioner. The HMB2 solver has a library of turbulence closures including several one- and two-equation turbulence models, and turbulence simulation is also possible using either the Large-Eddy or the Detached-Eddy simulation approach. The solver was designed with parallel execution in mind and the MPI library along with a load-balancing algorithm are used to this end. The flow solver can be used in serial or parallel fashion for large-scale problems. Depending on the purposes of the simulations, steady and unsteady wind turbine CFD simulations can be performed in HMB2 using single or full rotor meshes generated using the ICEM-Hexa tool. Rigid or elastic blades can be simulated using static or dynamic computations. HMB2 allows for sliding meshes to simulate rotor-tower interaction cases [6]. Alternatively, overset grids can be used [7]. To account for low-speed flows, the Low-Mach Roe scheme (LM-Roe) developed by Rieper [8,9] is employed for wind turbine cases.

For aero-elastic cases, the blade structure is modelled by a set of non-linear beam elements. The frequencies and shapes of the modes are obtained through NASTRAN [10] by performing a nonlinear static calculation. To account for the blade deformations, an aero-elastic method can be employed [11].

For static analysis, beam models are used and the loads per beam length are extracted at the location of the grid nodes of a NASTRAN FE model. The pressure is then integrated and loads are extracted as forces and moment per element length. These loads are applied to the NASTRAN model and a new blade shape is obtained. Finally, the mesh is deformed according to the new blade shape and new loads are calculated. This procedure is repeated until convergence in loads and blade shape is obtained.

For unsteady aero-elastic computation, the shape of the blade is expressed as a sum of eigenvectors, multiplied by their amplitudes. At each CFD solution update, the modal amplitudes are computed, the CFD grid is deformed, and the flow field is updated. At the end of each time step, the blade loads are extracted and re-applied to the system. This process is repeated until the end of the computation. For the grid deformation, the method of Dehaeze et al. [11] is used.

3. Results

Several numerical results are presented in this section. The section is organized by the type of computation including rigid or elastic blades, and blades equipped with the actuated leading and trailing edge flaps.

3.1 Rigid blades

First, steady and unsteady computations were preformed assuming rigid blades. The thrust and mechanical power as function of wind speed are presented in Figure 1. Steady computations of the flows without the tower were conducted to establish

this relation. The k-ω SST turbulence model was employed for all computations presented in this section. Two grids for each turbine were produced and denoted as coarse grid (CG) and fine grid (FG) in Figure 1. CG corresponds to 7M and 9.7M cells grids for InnWind and AVATAR blades, respectively. The cell spacing at the surface for coarse grids is $1 \cdot 10^{-5} C_{max}$, where C_{max} is a maximum chord of the blade – 6.206m for InnWind and 6.225m for AVATAR. FG corresponds to 9.2M and 9.7M cells grids for InnWind and AVATAR blades, respectively. The cell spacing at the surface for fine grids is $1 \cdot 10^{-6} C_{max}$. Figure 1 shows the HMB2 results for both wind turbines. For the rated wind speed and for lower speeds too, the HMB2 results agree reasonably with the design expectations. However, for the wind speeds above the nominal conditions HMB2 solution shows lower power than expected. This is due to the lack of any pitch input to increase the power and the fact that all computations were performed as fully-turbulent. Even if the flow Reynolds number can be very high for these wind turbines, still transition effects may be important. Further, the design pitch angle of the blade for all wind speeds was estimated based on the blade element momentum method [12,13].

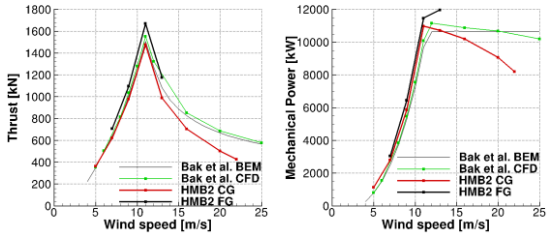

a) InnWind rotor

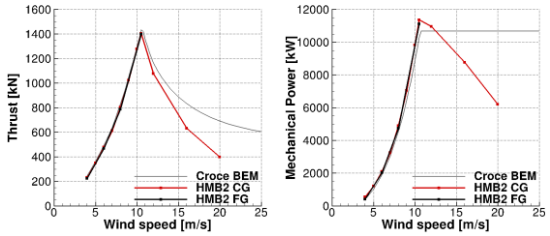

b) AVATAR rotor

Fig.1 Thrust force and mechanical power as function of wind speed for the InnWind (a) and AVATAR (b) rotors.

Unsteady computation was performed for the full configuration of the InnWind turbine. In this test case, blades have non-linear pre-bend of 3.3m and pre-cone of 2.5°. Additionally, the nacelle had an upward tilt of 5°, giving overall tower clearance of 18.3m. Baseline k-ω turbulence model and 20.4M cells grid with spacing at the surface of $1 \cdot 10^{-6} C_{max}$ were employed for this test case. Results of the computations are presented in Figure 2a in form of thrust and power as functions of azimuth angle. Clearly, the effect of the blade passing in front of the tower was captured. Figure 2b shows the iso-surface of Q=0.1 criterion at 810° of azimuth angle. Results obtained so far, suggest the deficit in thrust around 31.76kN (2.11%) and in power around 386.98kW (3.87%) for the InnWind turbine. The small relative variations of thrust and power are due to the large tower clearance.

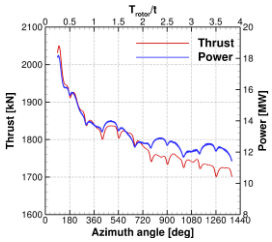

a) thrust and power

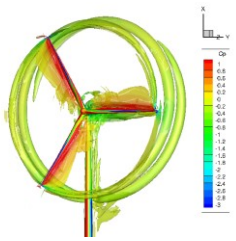

b) Iso-surface of Q=0.1 for InnWind turbine at 810° of azimuth angle

Fig.2 Thrust and power as function fo azimuth angle (a) and iso-surface of Q=0.1 at 810° of azimuth angle (b) for the complete InnWind turbine.

3.2 Elastic blades

Only the InnWind wind turbine [12] was investigated assuming elastic blades. The blade structure is modelled with a set of 50 non-linear, isotropic beam elements located at the shear centre of the blade. The elastic properties of each beam are set to match the flap-wise elastic properties computed by Bak et al. [12]. A CFD grid of 8.7M cells and the k-ω SST turbulence model were employed for this computation. The grid consisted of one, straight blade, and periodicity of the solution was assumed. Overall, 3 iterations between CFD and FEM were performed for a wind speed of 11m/s. The convergence history of the loads and blade shape is presented in Figure 3. The results indicate a tip displacement of 8.5m in the flap-wise direction, and 0.3m displacement in-plane. The final deformation of the blade for static aero-elastic computation is presented in Figure 4.

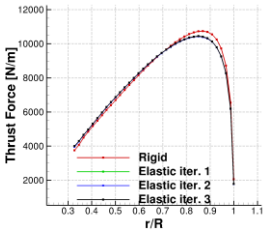

a) Thrust force

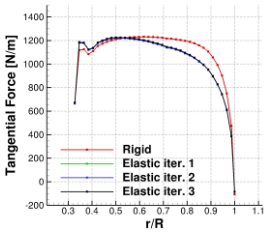

b) Tangential force

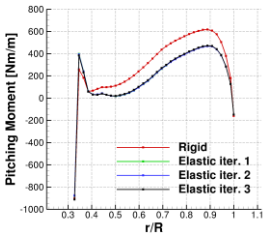

c) Pitching moment

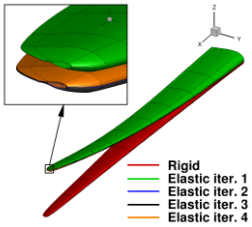

d) Blade shape

Fig.3 The convergence history of loads and blade shape for static aero-elastic analysis of InnWind blade.

For dynamic aero-elastic analysis, the shape of the blade is expressed as a sum of eigenvectors, multiplied by the excitation amplitudes, where the eigen-frequencies and eigen-modes are obtained from NASTRAN [11]. The blade structure is modelled with a set of 50 non-linear, isotropic beam elements located at the shear centre of the blade. The elastic properties of each beam are set to

match the flap-wise elastic properties computed by Bak et al. [12]. Also, the structural damping coefficients are set to match the values of [12].

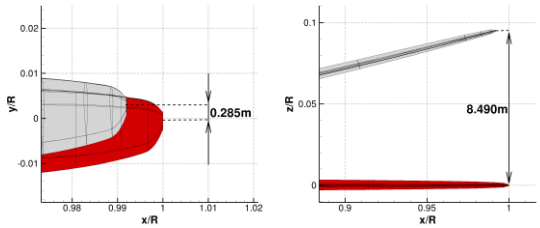

a) edge wise dispacement b) flap wise displacement

Fig.4 InnWind blade deformation for wind speed of 11m/s. Red – rigid, and grey – elastic blade.

The wind speed for this test case was 11m/s, and a mesh of 16.1M cells was used for the complete rotor. The k-ω SST turbulence model was employed. The tip displacements as function of the azimuth angle are presented in Figure 4a, and the thrust and power as functions of the azimuth angle are shown in Figure 4b. Figure 4c shows a comparison of the elastic and rigid blades at an azimuth angle of 320 degrees. The results show a tip displacement of 6.5m in the flap-wise direction and about 0.26m in-plane. The difference of 2m in the flap-wise displacement for static and dynamic aero-elastic computations stems from the different initial shape of the blade. For static analysis, the blade is straight, whereas for the dynamic computation, the blade had a pre-bending of 3.3m and a pre-coning of 2.5°. The dynamic flap-wise displacement reached 8.5m, and the tower clearance for the InnWind turbine was 18.3m. This indicates that a tower clearance of 10m would still be available.

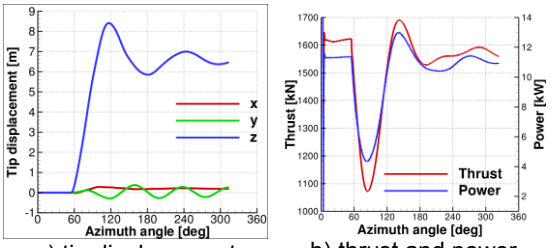

a) tip displacement b) thrust and power

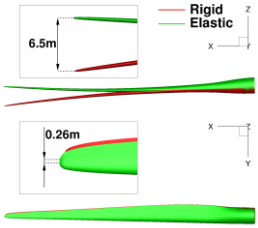

c) blade shape at azimuth angle 320 degrees

Fig.5 Results of dynamic aero-elastic computation. Tip displacement (a); thrust and power (b) as function of azimuth angle; and (c) the shape of the balde at 320° of azimuth angle.

3.3 Leading and trailing edge flaps

Both the InnWind and AVATAR blades in a straight configuration were equipped with leading and trailing edge flaps. The leading edge (LE) flap was located at 60%R station, and the trailing edge (TE) flap was located at 75%R. The length of each flap was 10%R, but the width of the TE flap was 10% of the local chord, whereas the width of the LE flap was 20% of the local chord, as shown in Figure 5a. The flaps are deflected form -10° to 10° with the shape and notation presented in Figure 5b.

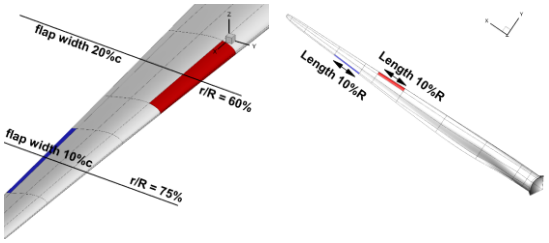

a) the location and dimentions of the trailing and leading edge flaps

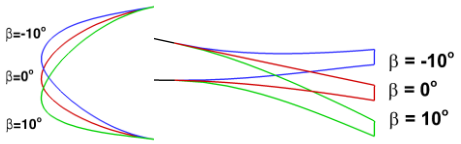

b) the shape of delfected LE and TE flaps

Fig.6 The definition of the flaps location and dimentions (a) and the shape and notaion for flap deflection (b).

Two frequencies of flap motion were studied – 0.16Hz (once per revolution) and 0.96Hz (six times per revolution). The inflow wind speed for both designs was 11.4m/s. The grid size was 9.2M and 9.7M cells for the InnWind and AVATAR blades, respectively. The cell spacing at the surface of the blade was $1 \cdot 10^{-6} C_{max}$, and the k-ω SST turbulence model is employed.

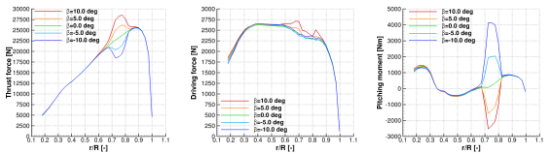

a) Trailing edge flap

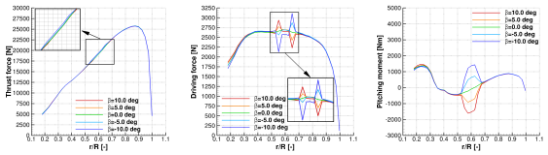

b) Leading edge flap

Fig.7 Spanwise destribution of thrust force, driving force and pitching moment for InnWind blade equipped with LE and TE flaps. Flap motion frequency f=0.96Hz.

The results for the InnWind wind turbine in form of span-wise load distributions are shown in Figure 7. The results for the AVATAR wind turbine are presented in Figures 8 and 9. As can be seen, the flap deflection has a localized effect on the loads distribution i.e. it does not affect the hole span of the blade. Further, the TE flap has a higher influence on thrust force, driving force and pitching moment, as compared to the LE flap. Also, the LE flap has the highest influence on the pitching moment, and a lesser influence on the tangential and normal forces.

Finally, a slightly wider variation of forces is obtained with a frequency of 0.96Hz as compared to 0.16Hz for the leading edge flap. Clearly, the actuated LE and TE flaps can be seen as a mechanism to locally change the loads acting on the blade.

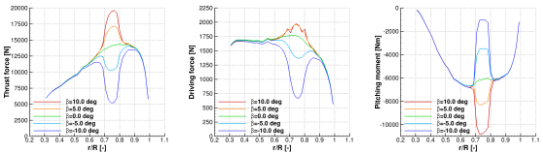

a) Trailing edge flap

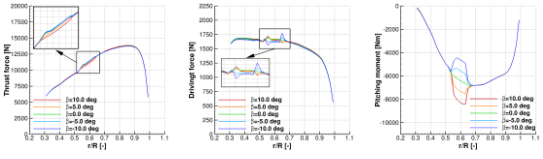

b) Leading edge flap

Fig.8 Spanwise destribution of thrust force, driving force and pitching moment for AVATAR blade equipped with LE and TE flaps. Flap motion frequency f=0.96Hz.

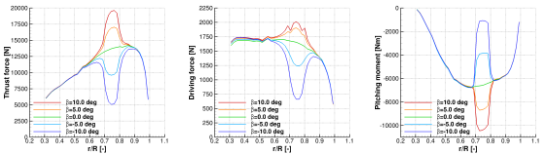

a) Trailing edge flap

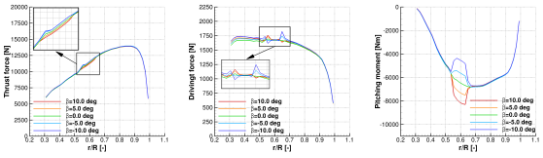

b) Leading edge flap

Fig.9 Spanwise destribution of thrust force, driving force and pitching moment for AVATAR blade equipped with LE and TE flaps. Flap motion frequency f=0.16Hz.

4. Conclusions

The paper presented results of numerical computations for two 10-MW wind turbines. The HMB2 CFD solver was used to compute the aerodynamic loads and blade shape. The blades were considered either rigid or elastic, where the estimated tip displacement for a latter case reached values of 8.5m. Both turbines were equipped with actuated leading and trailing edge flaps, and the load alleviation potential of such devices was investigated. The results show significant, but localized effect of the flap deflection on the distribution of the loads. The leading edge flap has a larger impact on the blade pitching moment than the leading edge flap. Further aero-elastic computations are planned in the near future.

Acknowledgements

The financial support of the Marie Curie Host Fellowships Program: FP7-PEOPLE-2012-ITN-309395 - "MARE-WINT" and the European Energy Research Alliance project: FP7-ENERGY-2013-1/no. 608396 - “AVATAR” are gratefully acknowledged.

5. References

[1] G.N. Barakos, R. Steijl, A. Brocklehurst and K. Badcock, Development of CFD Capability for Full Helicopter Engineering Analysis, 31st European Rotorcraft Forum, 2005.

[2] S. Gomez-Iradi, R. Steijl and G.N. Barakos, Development and Validation of a CFD Technique for the Aerodynamic Analysis of HAWT, Journal of Solar Energy Engineering-Transactions of the ASME, 131(3):031009, 2009. DOI: 10.1115/1.3139144.

[3] M. Carrión, M. Woodgate, R. Steijl, G. Barakos, S. Gomez-Iradi and X. Munduate, Computational Fluid Dynamics Analysis of the Wake behind the MEXICO Rotor in Axial Flow Conditions, Wind Energy, 2014, DOI: 10.1002/we.1745.

[4] http://www.innwind.eu/

[5] http://www.eera-avatar.eu/

[6] R. Steijl and G. Barakos, Sliding mesh algorithm for CFD analysis of helicopter rotorfuselage aerodynamics, International Journal for Numerical Methods in Fluids, Vol. 58, (5), 2008, pp. 527–549. DOI: 10.1002/fld.1757

[7] M. Jarkowski, M.A. Woodgate, G.N. Barakos and J. Rokicki, Towards consistent hybrid overset mesh methods for rotorcraft CFD, International Journal for Numerical Methods in Fluids, Vol. 74, (8), 2013, pp. 543–576. DOI: 10.1002/fld.3861

[8] F. Rieper, A low-Mach Number Fix for Roe’s Approximate Riemann Solver, J. Comput. Phys., Vol. 230, (13), June 2011, pp. 5263–5287. DOI: 10.1016/j.jcp.2011.03.025

[9] M. Carrión, M. Woodgate, R. Steijl and G. Barakos, Implementation of All-Mach Roe-type Schemes in Fully Implicit CFD Solvers – Demonstration for Wind Turbine Flows, International Journal for Numerical Methods in Fluids, Vol. 73, (8), 2013, pp. 693–728. DOI: 10.1002/fld.3818

[10] MSC.Software Corporation, MSC.Nastran 2005 Release Guide, Macmillan, 2005.

[11]F. Dehaeze and G.N. Barakos, Hovering Rotor Computations Using an Aeroelastic Blade Model, Aeronautical Journal, Vol. 116, Issue 1180, pp. 621-649, June 2012.

[12] C. Bak, F. Zhale, R. Bitsche, T. Kim, A. Yde, L.C. Henriksen, P.B. Andersen, A. Natarajan, M.H. Hansen, Description of the DTU 10 MW Reference Wind Turbine, Technical University of Denmark, DTU Wind Energy Report-I-0092, June 2013.

[13] A. Croce, Integration and Evaluation of 10MW Rotor, AVATAR project internal progress report